Alexandria Engineering Journal (2016) 55, 2229–2240

HOSTED BY

Alexandria University

Alexandria Engineering Journal

www.elsevier.com/locate/aej
www.sciencedirect.com

ORIGINAL ARTICLE

Hydromagnetic boundary layer flow of Williamson fluid in the presence of thermal radiation and Ohmic dissipation

T. Hayat [a,c], Anum Shafiq [a,b,*], A. Alsaedi [c]

[a] Department of Mathematics, Quaid-i-Azam University 45320, Islamabad 44000, Pakistan
[b] Department of Mathematics, Preston University Islamabad Campus, Pakistan
[c] Nonlinear Analysis and Applied Mathematics (NAAM) Research Group, Department of Mathematics, Faculty of Science, King Abdulaziz University, Jeddah 21589, Saudi Arabia

Received 26 January 2016; revised 23 May 2016; accepted 4 June 2016
Available online 4 July 2016

KEYWORDS

Viscous dissipation;
Thermal radiation;
Ohmic dissipation;
Williamson fluid;
Unsteady stretching

Abstract This paper is concerned with the unsteady two-dimensional boundary layer flow of an incompressible Williamson fluid over an unsteady permeable stretching surface with thermal radiation. Effects of electric and magnetic fields are considered. The nonlinear boundary layer partial differential equations are first converted into the system of ordinary differential equations and then solved analytically. Effects of physical parameters such as Weissenberg number, unsteadiness parameter, suction parameter, magnetic parameter, electric parameter, radiation parameter, Prandtl number and Eckert number on the velocity and temperature are graphically analyzed. The expressions of skin friction coefficient and local Nusselt number are presented and examined numerically.

1. Introduction

Magnetohydrodynamic (MHD) is a study of the interaction of electrically conducting fluids and electromagnetic forces. The MHD fluid was first introduced by Swedish Physicist, Alfven [1]. Hartman and Lazarus [2] studied the effects of a transverse uniform magnetic field in the flow of incompressible viscous fluid between two infinite insulating parallel plates. In recent years, the study of magnetohydrodynamic flow of an electrically conducting fluid past a heated surface has attracted the attention of many researchers. This is because of its considerable applications in many engineering problems such as plasma studies, petroleum industries, MHD power generators, cooling of nuclear reactors, the boundary layer control in aerodynamics and crystal growth. Extensive literature on the MHD flows in presence of applied magnetic field exists now. For example Rashidi et al. [3] considered the MHD flow of nanofluid induced by a rotating disk. Shahzad et al. [4] analyzed the hydromagnetic flow of Maxwell over a bidirectional stretching surface with variable thermal conditions. Turkyilmazoglu [5] analyzed the exact solution of magnetohydrodynamic viscous fluid by a rotating disk. Hayat et al. [6] discussed the buoyancy

* Corresponding author at: Department of Mathematics, Preston University Islamabad Campus, Pakistan.
E-mail address: anumshafiq@ymail.com (A. Shafiq).
Peer review under responsibility of Faculty of Engineering, Alexandria University.

http://dx.doi.org/10.1016/j.aej.2016.06.004

Nomenclature

u, v	axial and transverse velocity components (m/s)	T_w	surface temperature
x	axial coordinate (m)	T_∞	ambient temperature
y	transverse coordinate (m)	a, c	rate constants
ρ	density (kg m^{-3})	ψ	stream function
σ	electrical conductivity (m/s)	θ	dimensionless temperature
K	thermal conductivity (W K^{-1} m^{-1})	f	dimensionless velocity
T	temperature (K)	We	Weissenberg number
μ_0	viscosity (kg m^{-2} s^{-1})	M	magnetic parameter
υ	kinematic viscosity (m^2 s^{-1})	Ec	Eckert number
Γ	time constant	Re	Reynolds number
q_r	radiative heat flux	Pr	Prandtl number
c_p	specific heat (m^2 s^{-2})	E_1	local electric parameter
σ^*	Stefan-Boltzmann constant	A	dimensionless suction/injection parameter
$\mathbf{B}_0$	magnetic field	S	unsteadiness parameter
$\mathbf{J}$	joule current	R_d	radiation parameter
$\mathbf{E}_0$	electric field	τ_w	wall shear stress
k_1	mean absorption coefficient	q_w	rate of heat flux
U_w	stretching velocity	C_f	skin friction coefficient
V_w	suction/injection parameter	Nu_x	Nusselt number
T_0	reference temperature	$C_i (i = 1 - 5)$	constants

driven MHD flow of thixotropic fluid. They also examined the effects of thermophoresis and Joule heating in this investigation. An applied magnetic field effect in natural convection flow of nanofluid is studied by Sheikholeslami et al. [7]. Dandapat and Mukhopadhyay [8] discussed the stability characteristics of a thin conducting liquid film flowing and a non-conducting plane in the presence of electromagnetic field. Hayat et al. [9] investigated the series solution of magnetohydrodynamic axisymmetric flow of third grade fluid between porous disks with heat transfer. Unsteady magnetohydrodynamic mixed convection stagnation point flow of viscoelastic fluid towards a vertical surface is discussed by Ahmad and Nazar [10]. Magnetohydrodynamic Jeffery–Hamel nanofluid flow through non-parallel walls is investigated analytically by Hatami et al. [11]. They used different base fluids and nanoparticle. Sheikholeslami et al. [12] considered the effect of MHD in an inclined L-shape enclosure filled with nanofluid. Entropy analysis for a MHD nanofluid flow over a stretched surface is analyzed by Abolbashari et al. [13]. Rashidi et al. [14] made an analytical method for solving MHD convective and slip flow/-due to a rotating disk.

The effect of radiation on flow and heat transfer is important in the framework of space technology and processes involving high temperature. In the presence of a magnetic field, the radiative flows of an electrically conducting fluid with high temperature are encountered in electrical power generation, solar power technology, astrophysical flows, nuclear engineering applications and other industrial areas. The flows of viscous and non-Newtonian fluids through various aspects and thermal radiation have been examined by some researchers. For instance, Rashidi et al. [15] analytically studied the MHD mixed convective heat transfer in flow of incompressible viscoelastic fluid past a permeable wedge with thermal radiation. Bhattacharyya et al. [16] analyzed the effects of thermal radiation in micropolar fluid flow and heat transfer over a porous shrinking surface. Makinde and Ogulu [17] presented a numerical study for the effect of temperature dependent viscosity in free convective flow past a vertical porous plate. Here the influences of magnetic field, thermal radiation and a first order homogeneous chemical reaction are considered. Hayat et al. [18] investigated the effect of Joule heating in the flow of third-grade fluid over a radiative surface. Motsumi and Makinde [19] reported the numerical solutions for the effect of thermal radiation and viscous dissipation in boundary layer flow of nanofluids towards a permeable moving flat plate. Makinde [20] analyzed the hydromagnetic mixed convection heat and mass transfer flow of an incompressible Boussinesq fluid past a vertical porous plate with constant heat flux and thermal radiation. Shahzad et al. [21] studied the heat and mass transfer characteristics in three-dimensional flow of an Oldroyd-B fluid with thermal radiation.

The aim of present study wasand discussion are included to explore the hydromagnetics effects in the boundary layer flow of Williamson fluid over an unsteady permeable stretching sheet. Mathematical analysis has been carried out in presence of thermal radiation and Ohmic dissipation. This paper is structured as follows. The flow problem is formulated in Section two. Sections three and four deal with the series solutions and convergence analysis respectively. The series solutions are developed through homotopy analysis method [22–32]. Results and discussion are included in Section five and Section six consists of conclusions.

2. Mathematical formulation

Here the two-dimensional boundary layer flow of an incompressible electrically conducting Williamson fluid flow over unsteady porous stretching surface is considered. The flow is due to stretching sheet from a slit with the application of two equal and opposite forces in such a manner that the velocity field in flow direction is linear (see Fig. 1). Frictional heating in view of viscous dissipation is taken into account. The

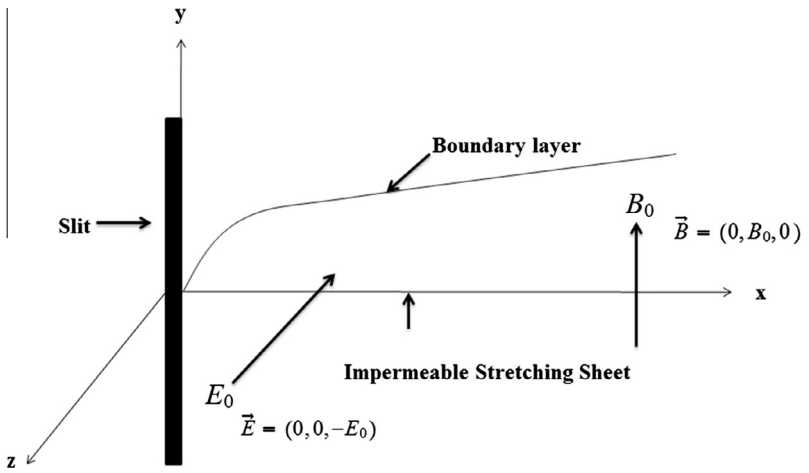

Figure 1 Physical model of boundary layer over a stretching sheet.

fluid considered has viscoelastic properties. The flow region is exposed by taking uniform transverse magnetic field $\vec{B} = (0, B_0, 0)$ and uniform electric field $\vec{E} = (0, 0, -E_0)$. The fluid subject to such fields is electrically conducting. Note that the magnetic field is weaker than the electric field and magnetic field obeys the Ohm's law $\tilde{\mathbf{J}} = \sigma\left(\vec{E} + \tilde{\mathbf{V}} \times \vec{B}\right)$, where $\tilde{\mathbf{J}}$ is the Joule current, σ is the electrical conductivity and $\tilde{\mathbf{V}}$ is the fluid velocity. The induced magnetic field and Hall effect are neglected. The relevant flow equations through conservation laws of mass, linear momentum and energy after using boundary layer approximations yield the following [18,33,34]:

$$\frac{\partial u}{\partial x} + \frac{\partial v}{\partial y} = 0, \tag{1}$$

$$\frac{\partial u}{\partial t} + u\frac{\partial u}{\partial x} + v\frac{\partial u}{\partial y} = v\frac{\partial^2 u}{\partial y^2} + 2v\Gamma\frac{\partial u}{\partial y}\frac{\partial^2 u}{\partial y^2} + \frac{\sigma}{\rho}\left(E_0 B_0 - B_0^2 u\right), \tag{2}$$

$$\rho c_p\left(\frac{\partial T}{\partial t} + u\frac{\partial T}{\partial x} + v\frac{\partial T}{\partial y}\right) = K\frac{\partial^2 T}{\partial y^2} + \mu_0\left(\frac{\partial u}{\partial y}\right)^2 + \mu_0\Gamma\left(\frac{\partial u}{\partial y}\right)^3 + \sigma(uB_0 - E_0)^2 - \frac{\partial q_r}{\partial y}. \tag{3}$$

Here u and v are the velocity components in the x and y directions respectively, ρ is the fluid density, σ is the electrical conductivity of fluid, K is the thermal conductivity, T is the temperature of fluid, c_p is the specific heat, v is the kinematic viscosity, Γ is the time constant and q_r is the radiative heat flux. By employing the Rosseland approximation, we have

$$q_r = -\frac{4\sigma^*}{3k_1}\frac{\partial T^4}{\partial y}, \tag{4}$$

where σ^* is the Stefan-Boltzmann constant and k_1 is the mean absorption coefficient. Through Taylor's series we have $T^4 \cong 4T_\infty^3 T - 3T_\infty^4$, where T_∞ is the ambient temperature and energy equation now reduces to the following expression:

$$\rho c_p\left(\frac{\partial T}{\partial t} + u\frac{\partial T}{\partial x} + v\frac{\partial T}{\partial y}\right) = \left(\frac{16\sigma^* T_\infty^3}{3k_1} + K\right)\frac{\partial^2 T}{\partial y^2} + \mu_0\left(\frac{\partial u}{\partial y}\right)^2 + \mu_0\Gamma\left(\frac{\partial u}{\partial y}\right)^3 + \sigma(uB_0 - E_0)^2. \tag{5}$$

The subjected boundary conditions for the present study are [18]

$$u(x,0) = U_w, v(x,0) = V_w, \quad T(x,0) = T_w,$$

$$u \to 0, \quad T \to T_\infty, \text{ as } y \to \infty, \tag{6}$$

where V_w is given by

$$V_w = -\frac{v_0}{(1-ct)^{1/2}}. \tag{7}$$

It expresses the mass transfer at surface with $V_w < 0$ for injection and $V_w > 0$ for suction. Moreover, the stretching velocity $U_w(x,t)$ and the surface temperature $T_w(x,t)$ are

$$U_w(x,t) = \frac{ax}{1-ct}, T_w(x,t) = T_\infty + T_0\frac{ax}{2v(1-ct)^2}, \tag{8}$$

in which a and c are the rate constants with $a > 0$ and $c \geqslant 0$ (i.e. $ct < 1$). The stream function is defined as

$$\eta = \sqrt{\frac{U_w}{xv}}y, \quad \psi = \sqrt{vxU_w}f(\eta), \quad \theta = \frac{T - T_\infty}{T_w - T_\infty}, \tag{9}$$

and the velocity components by

$$u = \frac{\partial\psi}{\partial y}, \quad v = -\frac{\partial\psi}{\partial x}. \tag{10}$$

Continuity equation is identically satisfied and the resulting problems of f and θ with associated boundary conditions can be expressed as follows:

$$f''' + ff'' - f'^2 - S\left\{f' + \frac{1}{2}\eta f'''\right\} + 2Wef''f''' + M^2\{E_1 - f'\} = 0, \tag{11}$$

$$\left(1 + \frac{4}{3}R_d\right)\theta'' + PrEcf''^2 - Pr\left[f'\theta - f\theta' + \frac{S}{2}\{\eta\theta' + 4\theta\}\right] + WePrEcf''^3 + M^2PrEc[f' - E_1]^2 = 0, \tag{12}$$

$$f(0) = A, \quad f'(0) = 1, \quad f'(\infty) \to 0, \quad f''(\infty) \to 0,$$
$$\theta(0) = 1, \quad \theta(\infty) \to 0. \tag{13}$$

The dimensionless parameters are defined as follows:

$$We = \Gamma U\sqrt{\frac{a}{v(1-ct)}}, \quad M^2 = \frac{\sigma B_0^2(1-ct)}{\rho a}, \quad E_1 = \frac{E_0(1-ct)}{B_0 ax}, \quad A = \frac{v_0}{\sqrt{av}}$$

$$S = \frac{c}{a}, \quad R_d = \frac{4\sigma^* T_\infty^3}{k^* K}, \quad Pr = \frac{\mu_0 c_p}{K}, \quad Ec = \frac{U_w^2}{c_p(T_w - T_\infty)}, \tag{14}$$

where We is the Weissenberg number, M is the magnetic parameter, E_1 is the local electric parameter, A is the suction parameter, S is the unsteadiness parameter, R_d is the radiation parameter, Pr is the Prandtl number and Ec is the Eckert number. Expression of skin friction coefficient is

$$C_f = \frac{\tau_w}{\rho U_w^2} = \frac{\tau_{xy}\big|_{y=0}}{\rho U_w^2}, \qquad Re_x^{1/2} C_f = \left[f''(0) + We f'^2(0)\right]. \tag{15}$$

The local Nusselt number is given by

$$Nu_x = \frac{x q_w}{K(T_w - T_\infty)} = -\frac{x\left(K + \frac{16\sigma^* T_\infty^3}{3k_1}\right)\frac{\partial T}{\partial y}\Big|_{y=0}}{K(T_w - T_\infty)},$$

$$Re_x^{-1/2} Nu_x = -\left(1 + \frac{4}{3}R_d\right)\theta'(0), \tag{16}$$

in which $Re_x = \frac{ax^2}{v(1-ct)}$ is the local Reynolds number.

3. Analytical solutions

The velocity $f(\eta)$ and the temperature $\theta(\eta)$ can be expressed in the form of base functions

$$\left\{\eta^k \exp(-n\eta)\middle| k \geqslant 0, n \geqslant 0\right\} \tag{17}$$

as follows:

$$f_m(\eta) = \sum_{n=0}^{\infty}\sum_{k=0}^{\infty} a_{m,n}^k \eta^k \exp(-n\eta), \tag{18}$$

$$\theta_m(\eta) = \sum_{n=0}^{\infty}\sum_{k=0}^{\infty} b_{m,n}^k \eta^k \exp(-n\eta), \tag{19}$$

where $a_{m,n}^k$ and $b_{m,n}^k$ are the coefficients. Invoking the rule of solution expressions, the initial guesses f_0 and θ_0 and the auxiliary linear operators are

$$f_0(\eta) = A + 1 - \exp(-\eta), \quad \theta_0(\eta) = \exp(-\eta), \tag{20}$$

$$\mathcal{L}(f) = \frac{d^3 f}{d\eta^3} - \frac{df}{d\eta}, \quad \mathcal{L}(\theta) = \frac{d^2\theta}{d\eta^2} - \theta, \tag{21}$$

satisfying the following properties:

$$\mathcal{L}_f[C_1 + C_2 \exp(\eta) + C_3 \exp(-\eta)] = 0, \tag{22}$$

$$\mathcal{L}_\theta[C_4 \exp(\eta) + C_5 \exp(-\eta)] = 0, \tag{23}$$

in which $C_i (i = 1-5)$ depict the arbitrary constants. If $p \in [0,1]$ is the embedding parameter, $\hbar_f$ and $\hbar_\theta$ are the non-zero auxiliary parameters, then zeroth order deformation problems are constructed in the following forms:

$$(1-p)\mathcal{L}_f[\hat{f}(\eta,p) - f_0(\eta)] = p\hbar_f \mathcal{N}_f\left[\hat{f}(\eta,p)\right], \tag{24}$$

$$(1-p)\mathcal{L}_\theta[\hat{\theta}(\eta,p) - \theta_0(\eta)] = p\hbar_\theta \mathcal{N}_\theta\left[\hat{f}(\eta,p), \hat{\theta}(\eta,p)\right], \tag{25}$$

$$\hat{f}(\eta;p)\Big|_{\eta=0} = A, \quad \frac{\partial \hat{f}'(\eta;p)}{\partial\eta}\bigg|_{\eta=0} = 1, \quad \frac{\partial \hat{f}'(\eta;p)}{\partial\eta}\bigg|_{\eta=\infty} = 0,$$

$$\hat{\theta}(\eta;p)\Big|_{\eta=0} = 1, \quad \hat{\theta}(\eta;p)\Big|_{\eta=\infty} = 0. \tag{26}$$

The corresponding non-linear operators $\mathcal{N}_f\left[\hat{f}(\eta,p)\right]$ and $\mathcal{N}_\theta\left[\hat{f}(\eta,p), \hat{\theta}(\eta,p)\right]$ are given below:

$$\begin{aligned}\mathcal{N}_f\left[\hat{f}(\eta;p)\right] = {} & \frac{\partial^3 \hat{f}(\eta,p)}{\partial\eta^3} - \left(\frac{\partial \hat{f}(\eta,p)}{\partial\eta}\right)^2 + \hat{f}(\eta,p)\frac{\partial^2 \hat{f}(\eta,p)}{\partial\eta^2} \\ & - S\left\{\frac{\partial \hat{f}(\eta,p)}{\partial\eta} + \frac{1}{2}\eta\frac{\partial^2 \hat{f}(\eta;q)}{\partial\eta^2}\right\} \\ & + 2We\frac{\partial^2 \hat{f}(\eta;q)}{\partial\eta^2}\frac{\partial^3 \hat{f}(\eta;q)}{\partial\eta^3} + M^2\left\{E_1 - \frac{\partial \hat{f}(\eta,p)}{\partial\eta}\right\},\end{aligned} \tag{27}$$

$$\begin{aligned}\mathcal{N}_\theta\left[\hat{f}(\eta;p), \hat{\theta}(\eta;p)\right] = {} & \left(1 + \frac{4}{3}R_d\right)\frac{\partial^2 \hat{\theta}(\eta;p)}{\partial\eta^2} + PrEc\left(\frac{\partial^2 \hat{f}(\eta,p)}{\partial\eta^2}\right)^2 \\ & - Pr\left[\frac{S}{2}\left\{4\theta + \eta\frac{\partial \hat{\theta}(\eta;p)}{\partial\eta}\right\} + \frac{\partial \hat{f}(\eta;q)}{\partial\eta}\hat{\theta}(\eta;p)\right. \\ & \left. - \hat{f}(\eta,p)\frac{\partial \hat{\theta}(\eta;p)}{\partial\eta}\right] + WePrEc\left(\frac{\partial^2 \hat{f}(\eta,p)}{\partial\eta^2}\right)^3 \\ & + M^2 PrEc\left[\frac{\partial \hat{f}(\eta;q)}{\partial\eta} + E_1\right]^2.\end{aligned} \tag{28}$$

For $p = 0$ and $p = 1$, one can write

$$\hat{f}(\eta;0) = f_0(\eta), \quad \hat{\theta}(\eta;0) = \theta_0(\eta),$$

$$\hat{f}(\eta;1) = f(\eta), \quad \hat{\theta}(\eta;1) = \theta(\eta). \tag{29}$$

If p increases from 0 to 1, $\hat{f}(\eta;p)$ and $\hat{\theta}(\eta;p)$ deform from the initial solutions $f_0(\eta)$ and $\theta_0(\eta)$ to the final solutions $f(\eta)$ and $\theta(\eta)$ respectively. Using Taylor series, we have

$$\hat{f}(\eta;p) = f_0(\eta) + \sum_{m=1}^{\infty} f_m(\eta)p^m, \qquad f_m(\eta) = \frac{1}{m!}\frac{\partial^m \hat{f}(\eta;p)}{\partial p^m}\bigg|_{p=0}, \tag{30}$$

$$\hat{\theta}(\eta;p) = \theta_0(\eta) + \sum_{m=1}^{\infty} \theta_m(\eta)p^m, \qquad \theta_m(\eta) = \frac{1}{m!}\frac{\partial^m \hat{\theta}(\eta;p)}{\partial p^m}\bigg|_{p=0}. \tag{31}$$

Note that the auxiliary parameters are properly chosen such that the series (30) and (31) converge at $p = 1$. Therefore

$$f(\eta) = f_0(\eta) + \sum_{m=1}^{\infty} f_m(\eta), \tag{32}$$

$$\theta(\eta) = \theta_0(\eta) + \sum_{m=1}^{\infty} \theta_m(\eta). \tag{33}$$

The mth-order deformation problems can be expressed as follows:

$$\mathcal{L}_f[f_m(\eta)-\chi_m f_{m-1}(\eta)]=\hbar_f\mathcal{R}_m^f(\eta), \tag{34}$$

$$\mathcal{L}_\theta[\theta_m(\eta)-\chi_m\theta_{m-1}(\eta)]=\hbar_\theta\mathcal{R}_m^\theta(\eta), \tag{35}$$

$$\hat{f}_m(\eta;p)\Big|_{\eta=0}=0,\quad \frac{\partial\hat{f}'_m(\eta;p)}{\partial\eta}\Big|_{\eta=0}=0,\quad \frac{\partial\hat{f}'_m(\eta;p)}{\partial\eta}\Big|_{\eta=\infty}=0,$$

$$\hat{\theta}_m(\eta;p)\Big|_{\eta=0}=0,\hat{\theta}_m(\eta;p)\Big|_{\eta=\infty}=0, \tag{36}$$

$$\begin{aligned}\mathcal{R}_m^f(\eta)=&f'''_{m-1}(\eta)+\sum_{k=0}^{m-1}\left(f_{m-1-k}f''_k-f'_{m-1-k}f'_k\right)\\&-S\left(f'_{m-1}+\frac{1}{2}\eta f''_{m-1}\right)+2We\sum_{k=0}^{m-1}f''_{m-1-k}f'''_k\\&+M^2\left[E_1(1-\chi_m)-f'_{m-1}\right],\end{aligned} \tag{37}$$

$$\begin{aligned}\mathcal{R}_m^\theta(\eta)=&\left(1+\frac{4}{3}R_d\right)\theta''_{m-1}\\&-Pr\left[\sum_{k=0}^{m-1}f'_{m-1-k}\theta_k-\sum_{k=0}^{m-1}f_{m-1-k}\theta'_k+\frac{S}{2}\{\eta\theta'_{m-1}+4\theta_{m-1}\}\right]\\&+PrEc\sum_{k=0}^{m-1}f''_{m-1-k}f''_k\\&+WePrEc\sum_{k=0}^{m-1}f''_{m-1-k}\sum_{l=0}^{k}f''_{k-l}f''_l\\&+M^2PrEc\left[f'_{m-1}-E_1(1-\chi_m)\right]^2,\end{aligned} \tag{38}$$

$$\chi_m=\begin{cases}0, & m\leqslant 1,\\ 1, & m>1.\end{cases} \tag{39}$$

The general solutions of Eqs. (34)–(36) in terms of special solutions (f_m^*,θ_m^*) are given by

$$f_m(\eta)=f_m^*(\eta)+C_1+C_2\exp(\eta)+C_3\exp(-\eta),$$
$$\theta_m(\eta)=\theta_m^*(\eta)+C_4\exp(\eta)+C_5\exp(-\eta).$$

4. Convergence of the derived solutions

The expressions given in (32) and (33) have the non-zero auxiliary parameters $\hbar_f$ and $\hbar_\theta$. The auxiliary parameters are efficient in adjusting and controlling the convergence. To obtain the meaningful ranges of these parameters, the $\hbar_f$ and $\hbar_\theta$-curves are plotted up to 10^{th} order of approximation given in Fig. 2. By looking at the range of parameters the decisive values of $\hbar_f$ and $\hbar_\theta$ are $-1.5\leqslant\hbar_f<-0.53$ and $-1.35\leqslant\hbar_\theta<-0.4$. Moreover, the convergence of series solutions is analyzed and shown in Table 1. This can be seen from Table 1 that series solutions converge up to 24th order of approximation for velocity and 40th order of approximation for temperature up to 4 decimal places.

5. Results and discussion

To observe the influences of all physical parameters on the velocity and temperature profiles, the graphs are displayed in Figs. 3–25. The numerical values of skin friction coefficient $Re_x^{1/2}C_f$ and the local Nusselt number $Re_x^{-1/2}Nu_x$ are presented in Tables 2 and 3.

Fig. 3 is drawn to observe the influence of magnetic parameter on the velocity $f'(\eta)$ versus η. It is worth mentioning that the velocity distribution decreases for the larger values of the magnetic parameter M. In addition, the momentum boundary layer thickness is reduced. Physically, increase in magnetic force results in the enhancement of the Lorentz force which resists the fluid flow. Consequently there is a decrease in the velocity profile. Fig. 4 shows the variation of Weissenberg number We on the velocity $f'(\eta)$ via η. It is found that the velocity and momentum boundary layer thickness decrease near the wall with an increased value of We. However it vanishes away from the wall. Fig. 5 is sketched for the effect of suction parameter A on the velocity profile $f'(\eta)$. The velocity field decays near the wall and it almost vanishes away from the wall. There is also a reduction in the momentum boundary layer thickness. The similar characteristics are observed in Fig. 6 for unsteadiness parameter on the velocity profile $f'(\eta)$. The behavior of the electric parameter E_1 on the velocity $f'(\eta)$ is presented in Fig. 7. We examined that the momentum boundary layer increases near the wall with very small rate for the larger values of the electric parameter E_1 while it increases more rapidly away from the stretching surface. This analysis reveals that the effect of electric parameter is to shift the streamlines away from the stretched boundary. It is because of Lorentz force which reduces the frictional resistance.

Figs. 8 and 9 display the effect of magnetic parameter M and Weissenberg number We on the temperature profile $\theta(\eta)$. It is noted that the temperature profile increases near the wall at the small rate whereas it rises more rapidly for the region $0.5\leqslant\eta\leqslant2.5$ and it almost vanishes for $\eta>2.5$. The variation of temperature distribution with the change of Weissenberg number We is predicted in Fig. 9. A reduction of temperature profile $\theta(\eta)$ and the thermal boundary layer

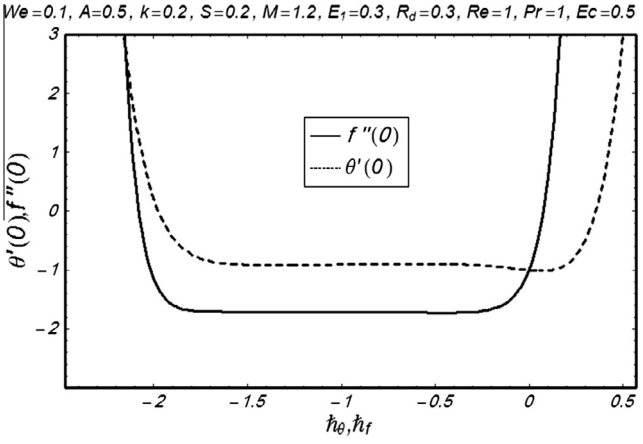

Figure 2 $\hbar$-curves of $f''(0)$ and $\theta'(0)$ at 10th order of approximation.

Table 1 Convergence of homotopy solutions when $We = 0.1$, $S = 0.2, A = 0.3, E_1 = 0.3, R_d = 0.3, M = 0.1, Pr = 1,$ and $Ec = 0.5$.

Order of approximation	$-f''(0)$	$-\theta'(0)$
1	1.272	0.9338
5	1.541	0.8597
10	1.563	0.8555
24	1.551	0.8662
30	1.551	0.99211
40	1.551	0.99051
50	1.551	0.99051

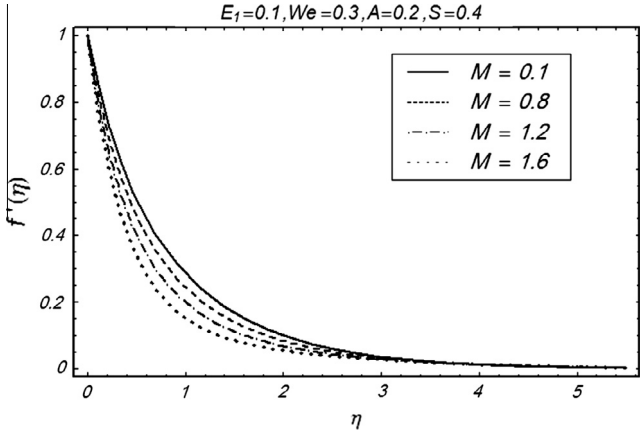

Figure 3 Variation of velocity component $f'(\eta)$ versus η for magnetic parameter M.

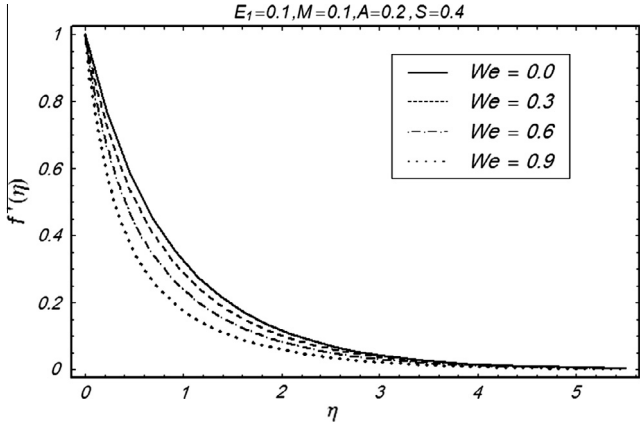

Figure 4 Variation of velocity component $f'(\eta)$ versus η for Weissenberg number We.

thickness is observed. The temperature profile $\theta(\eta)$ for various values of suction parameter A is plotted in Fig. 10. It is apparent that an increase in suction parameter A reduces the temperature profile $\theta(\eta)$ and thermal boundary layer thickness. Fig. 11 is presented to examine the effect of unsteadiness parameter S on the temperature profile $\theta(\eta)$. The temperature profile and the thermal boundary layer are decreased near the

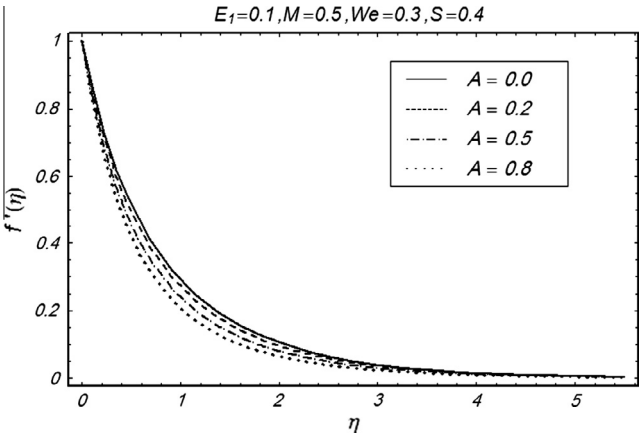

Figure 5 Variation of velocity component $f'(\eta)$ versus η for suction parameter A.

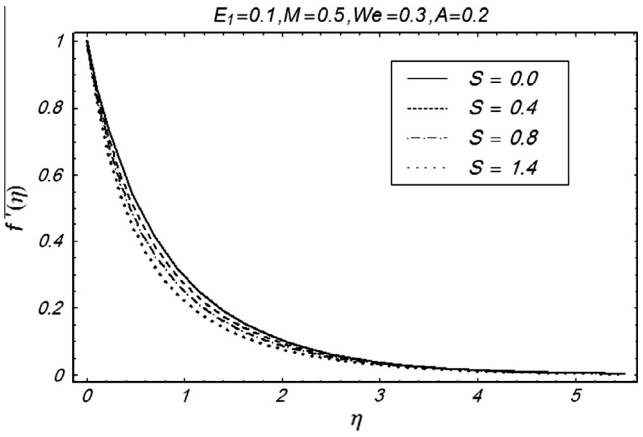

Figure 6 Variation of velocity component $f'(\eta)$ versus η for unsteadiness parameter S.

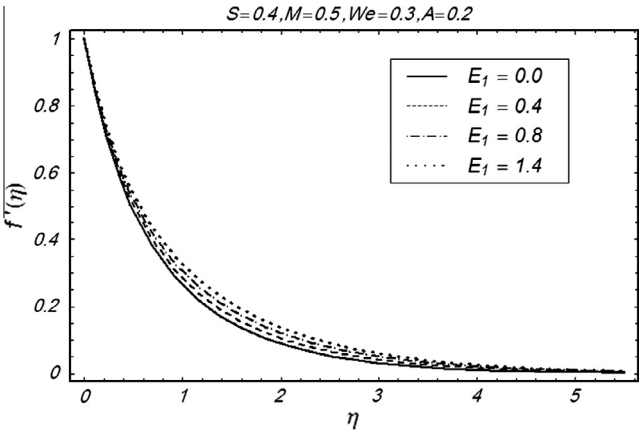

Figure 7 Variation of velocity component $f'(\eta)$ versus η for electric parameter E_1.

wall while it drops out of the sight of the stretching plate. The fluctuation of the radiation parameter R_d on temperature distribution is seen in Fig. 12. Study of the graph shows that the effect of radiation parameter R_d shows an increase in both the

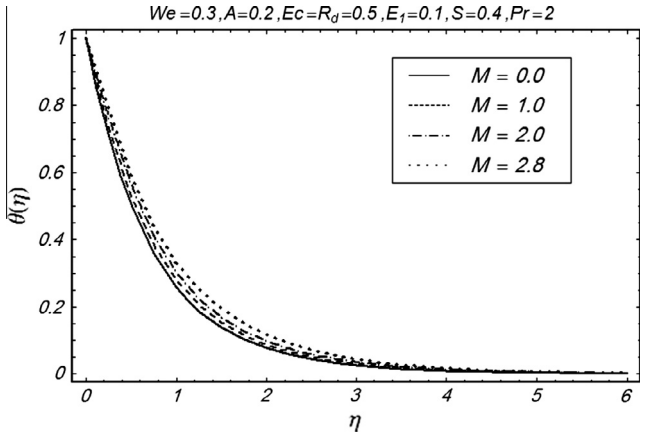

Figure 8 Dimensionless temperature profile $\theta(\eta)$ versus η for magnetic parameter M.

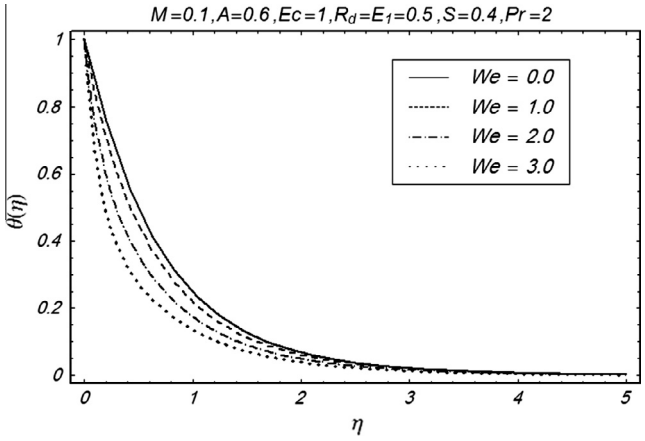

Figure 9 Dimensionless temperature profile $\theta(\eta)$ versus η for various values of Weissenberg number We.

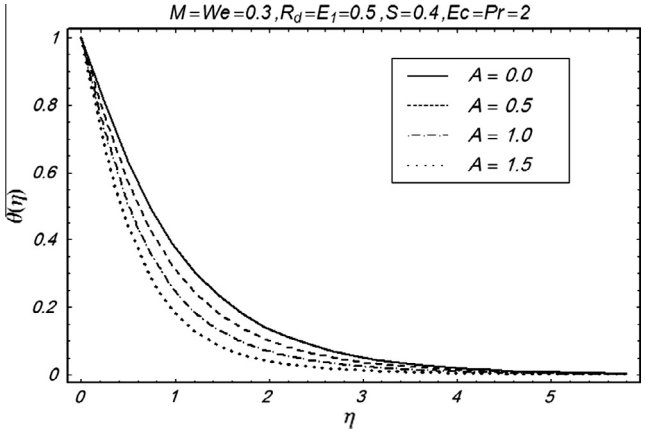

Figure 10 Dimensionless temperature profile $\theta(\eta)$ versus η for various values of suction parameter A.

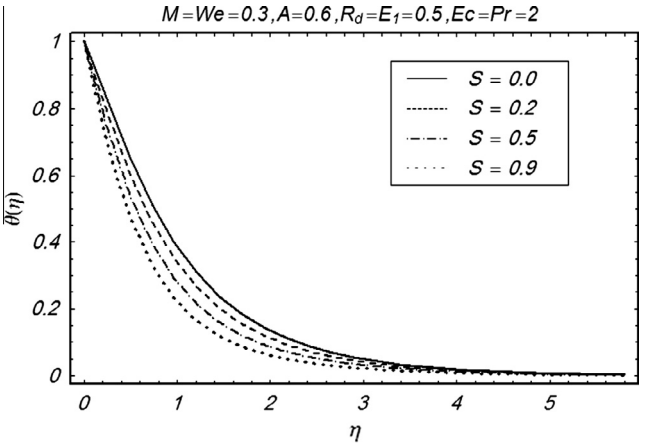

Figure 11 Dimensionless temperature profile $\theta(\eta)$ versus η for various values of unsteadiness parameter S.

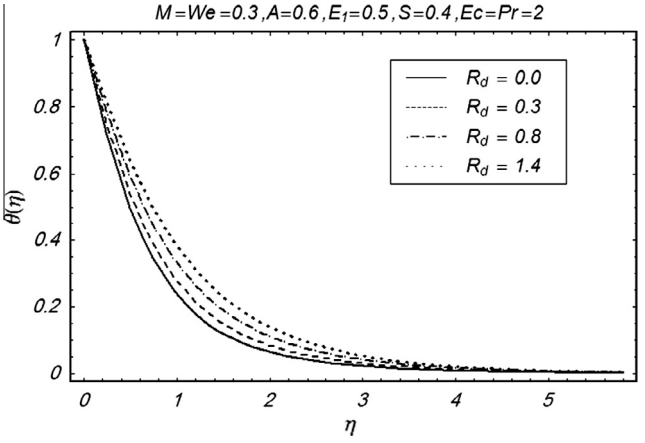

Figure 12 Dimensionless temperature profile $\theta(\eta)$ versus η for various values of radiation parameter R_d.

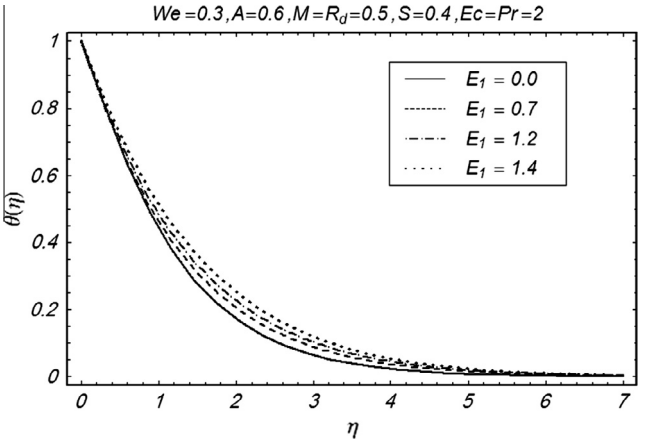

Figure 13 Dimensionless temperature profile $\theta(\eta)$ versus η for various values of E_1.

temperature profile $\theta(\eta)$ and the thermal boundary layer thickness. Fig. 13 describes that there is higher temperature and the higher thermal boundary layer thickness for the larger values of the electric parameter E_1. It is examined that the temperature profile near the wall increases with small rate. Additionally it increases immediately away from the wall and it disappears near to $\eta \geqslant 6$. Figs. 14 and 15 exhibit the outcomes

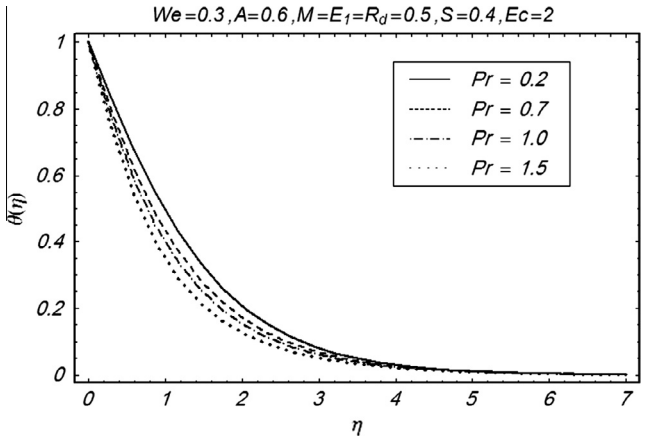

Figure 14 Dimensionless temperature profile $\theta(\eta)$ versus η for various values of Prandtl number Pr.

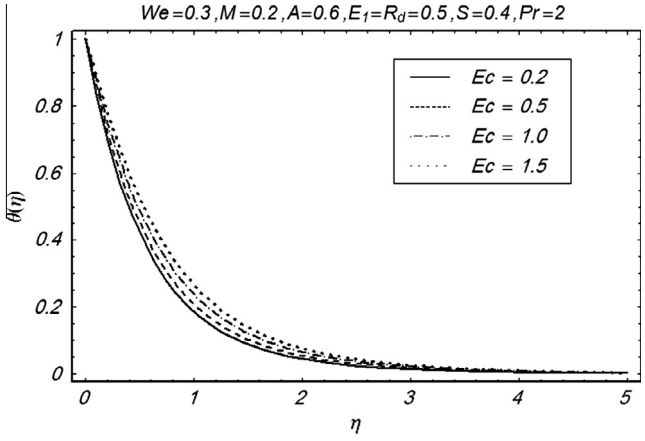

Figure 15 Dimensionless temperature profile $\theta(\eta)$ versus η for various values of Eckert number Ec.

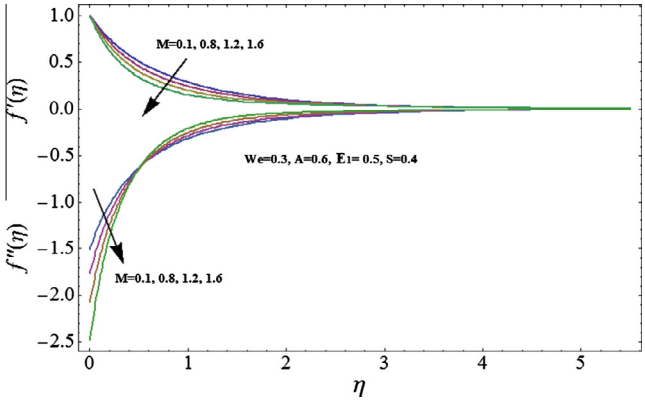

Figure 16 Variations of velocity $f'(\eta)$ and $f''(\eta)$ versus η for several values of magnetic parameter M.

of Prandtl number Pr and Eckert number Ec on the temperature profile. The temperature profile and the thermal boundary layer are reduced with an increase in Prandtl number Pr. From Fig. 14 it is very clear that the Prandtl number indicates the ratio of momentum diffusivity to the thermal diffusivity.

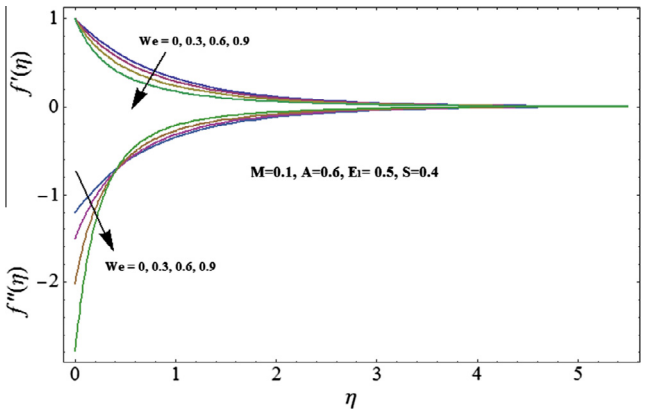

Figure 17 Variations of velocity $f'(\eta)$ and $f''(\eta)$ versus η for several values of Weissenberg number We.

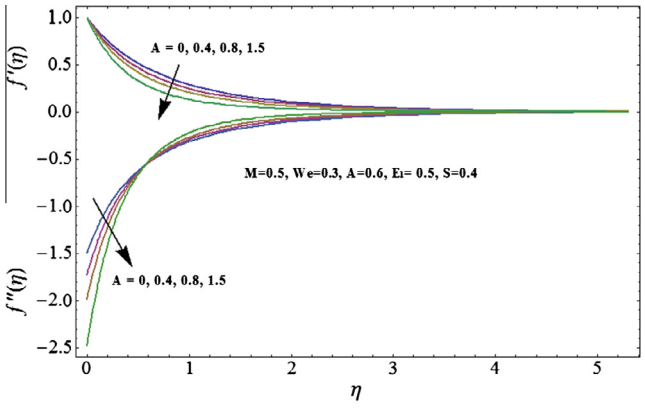

Figure 18 Variations of velocity $f'(\eta)$ and $f''(\eta)$ versus η for several values of suction parameter A.

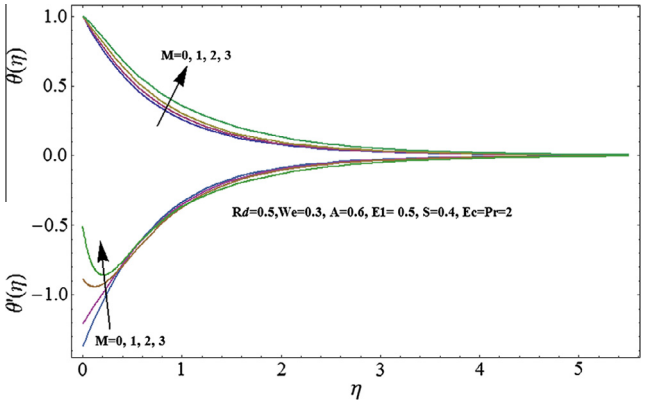

Figure 19 Variations of temperature $\theta(\eta)$ and temperature gradient $\theta'(\eta)$ versus η for several values of magnetic parameter M.

Therefore Prandtl number Pr controls the relative thickening of the momentum and the thermal boundary layer in the heat transfer process. Fig. 15 represents the graph of temperature profile for various values of Eckert number Ec. Due to the frictional heating, the thermal boundary layer thickness is increased through the influence of Eckert number.

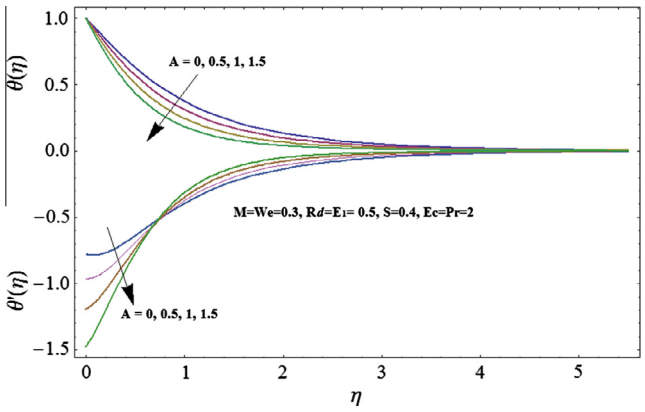

Figure 20 Variations of temperature $\theta(\eta)$ and temperature gradient $\theta'(\eta)$ versus η for several values of suction parameter A.

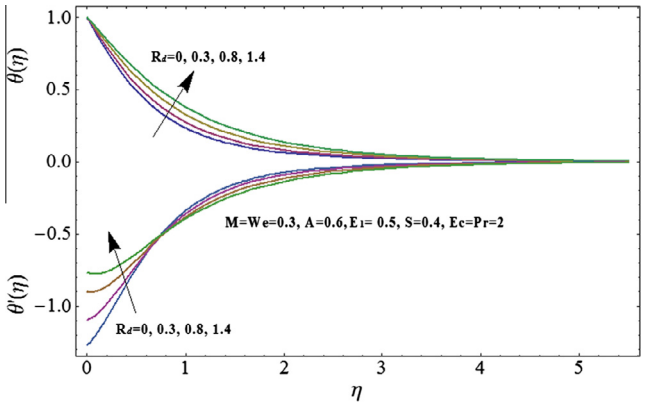

Figure 21 Variations of temperature $\theta(\eta)$ and temperature gradient $\theta'(\eta)$ versus η for several values of radiation parameter R_d.

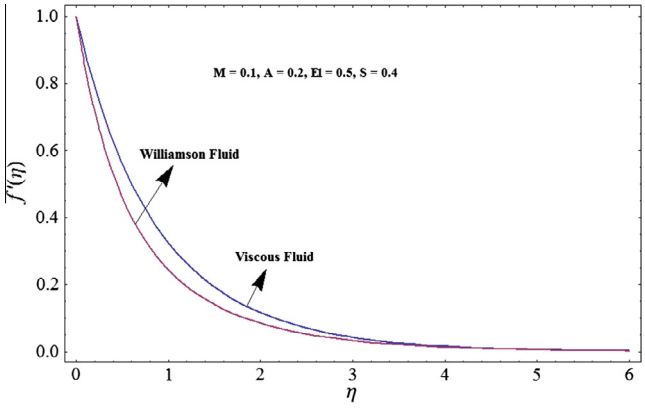

Figure 22 Velocity profiles for viscous and Williamson fluids.

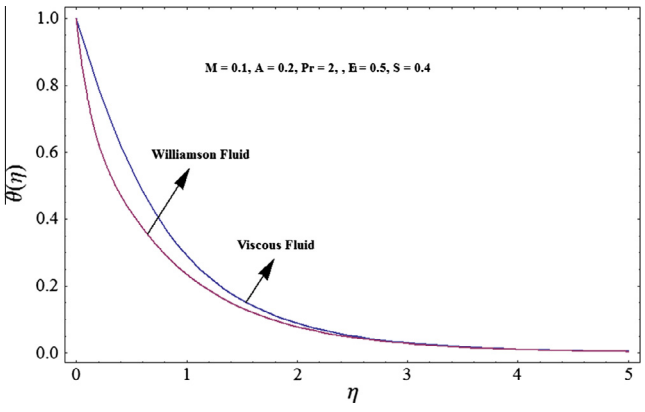

Figure 23 Temperature profiles for viscous and Williamson fluids.

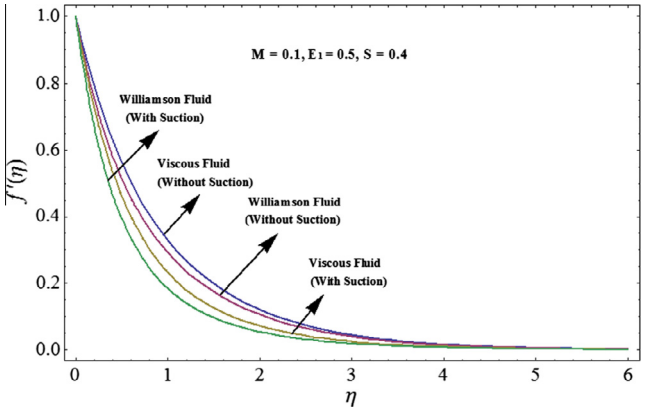

Figure 24 Velocity profiles with and without suction for viscous and Williamson fluids.

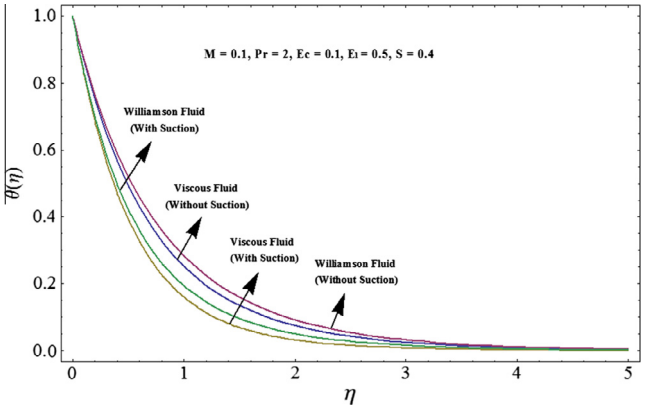

Figure 25 Temperature profiles with and without suction for viscous and Williamson fluids.

Fig. 16 represents the effects of magnetic parameter M on the velocity $f'(\eta)$ and $f''(\eta)$. Initially when there is no effect of the magnetic parameter at the edge then the velocity is maximum at $\eta = 0$. The velocity profile decreases near the wall and it vanishes far away from the wall when the magnetic parameter M is increased. On the other hand $f''(\eta)$ decreases near the wall and has opposite behavior in the region $0.5 \leqslant \eta \leqslant 2$ and eventually approaches to zero. Fig. 16 illustrates that $f''(\eta)$ at the wall is negative. Physically, it means that the surface exerts a drag force on the fluid particle and the reverse sign implies the opposite. Fig. 17 is plotted to investigate the effect of Weissenberg number We on the velocity $f'(\eta)$ and

Table 2 Numerical values of skin friction coefficients $Re_x^{1/2}C_f$ for different values of physical parameters.

We	A	S	M	E_1	$-Re_x^{1/2}C_f$
0.1	0.2	0.2	0.7	0.1	1.271
0.2					1.177
0.23					1.087
0.1	0.2	0.2	0.7	0.1	1.271
	0.3				1.321
	0.4				1.373
0.1	0.2	0.2	0.7	0.1	1.271
		0.3			1.298
		0.4			1.324
0.1	0.2	0.2	0.7	0.1	1.271
			0.8		1.314
			0.9		1.359
0.1	0.2	0.2	0.7	0.1	1.271
				0.2	1.234
				0.3	1.197

the $f''(\eta)$. It is revealed that the velocity profile is decreasing function of Weissenberg number We. It decreases more rapidly near the wall and approaches to zero away from the wall. The $f''(\eta)$ near the wall decreases at higher rate whereas it has reverse behavior for $0.5 < \eta < 2.5$ and has merging behavior for $\eta > 2.5$. The graph of velocity field $f'(\eta)$ for various values of suction parameter A is drawn in Fig. 18. The horizontal velocity attains maximum value at $\eta = 0$ for all values of suction parameter A and it decreases with high rate by increasing value of η and finally it vanishes. The magnitude of $f''(\eta)$ is an increasing function of suction parameter A. This is because of the drag force which the surface applied on the fluid. Variations of dimensionless temperature $\theta(\eta)$ and the temperature gradient $\theta'(\eta)$ for different values of magnetic parameter are shown in Fig. 19. Temperature increases with increasing magnetic parameter M, whereas the same behavior is noted for the temperature gradient near the wall and has reversed behavior for $0.5 < \eta < 3$ and finally vanishes for larger values of η. Fig. 20 elucidates the effect of suction parameter A on the temperature $\theta(\eta)$ and the temperature gradient $\theta'(\eta)$. Here the temperature is decreasing function of A. Also we noted that the magnitude of temperature gradient increases near the wall and for some values of η it shows the decreasing behavior. Effect of radiation parameter R_d on the temperature profile $\theta(\eta)$ and the temperature gradient $\theta'(\eta)$ is displayed in Fig. 21. The temperature profile is increasing function of R_d. As the radiation is an external source which causes to increase the fluid temperature the magnitude of the temperature gradient $\theta'(\eta)$ is decreasing function of radiation parameter R_d. The opposite behavior is seen in the region $0.8 \leqslant \eta \leqslant 3$ and ultimately it vanishes away from the wall when $\eta > 3$. Fig. 22 is displayed for the velocity comparison of viscous fluid and the Williamson fluid. It is observed that the velocity is higher in case of viscous fluid when compared with the Williamson fluid. Fig. 23 is plotted for the comparative study of temperature in the viscous and Williamson fluids. It is found that the temperature field is greater for viscous fluid than Williamson fluid. Fig. 24 represents the comparison of velocity profile with and without suction for viscous and Williamson fluids. It can be seen from this figure that viscous fluid has higher velocity profile in comparison with the Williamson fluid. This observation holds in presence/absence of suction. It is also noted that the velocity in absence of suction is more than the presence of suction for both viscous and Williamson fluid cases. Fig. 25 demonstrates that temperature distribution for Williamson fluid case is higher in absence of suction. Numerical values of skin friction coefficient $Re_x^{1/2}C_f$ for different values of Weissenberg number We, suction parameter A, unsteadiness parameter S, magnetic parameter M and electric parameter E_1 are computed in Table 2. Analysis of the Table shows that suction parameter A, unsteadiness parameter S and magnetic parameter M rise the rate of wall shear stress. Hence the rate of wall shear stress can be reduced for the smaller values of the suction parameter A, unsteadiness parameter S and magnetic parameter M. On the other hand the effect of Weissenberg number We and the electric parameter E_1 reduced the rate of wall shear stress. Therefore the larger values of We and E_1 can be used to decrease the rate of wall shear stress. Table 3 presents the numerical values of local Nusselt number for various values of Weissenberg number We, suction parameter A, unsteadiness parameter S, magnetic parameter M and electric parameter E_1. Tabulated values show that the effect of suction parameter A, unsteadiness parameter S, electric parameter E_1 and Prandtl number Pr enhances the rate of heat transfer across the stretching sheet to the fluid. Since the rate of heat transfer is higher for larger values of A, S, E_1 and Pr, these parameters can be used as the cooling factor. However the rate of heat transfer is reduced for the larger values of

Table 3 Numerical values of Nusselt number $Re_x^{-1/2}Nu_x$ for different values of physical parameters.

We	A	S	M	E_1	R_d	Pr	Ec	$Re_x^{-1/2}Nu_x$
0.1	0.2	0.2	0.7	0.1	0.3	1	0.5	0.7962
0.2								0.7872
0.3								0.7212
0.1	0.2	0.2	0.7	0.1	0.3	1	0.5	0.7962
	0.3							0.8237
	0.4							0.8516
0.1	0.2	0.2	0.7	0.1	0.3	1	0.5	0.7962
		0.3						0.8669
		0.4						0.9314
0.1	0.2	0.2	0.7	0.1	0.3	1	0.5	0.7962
			0.8					0.7752
			0.9					0.7520
0.1	0.2	0.2	0.7	0.1	0.3	0.1	0.5	0.7962
				0.2				0.8287
				0.3				0.8614
0.1	0.2	0.2	0.7	0.1	0.3	1	0.5	0.7962
					0.4			0.7582
					0.5			0.7248
0.1	0.2	0.2	0.7	0.1	0.3	1	0.5	0.7962
						1.1		0.8382
						1.2		0.8782
0.1	0.2	0.2	0.7	0.1	0.3	1	0.5	0.7962
							0.6	0.7541
							0.7	0.7120

the Weissenberg number We, magnetic parameter M, radiation parameter R_d and the Eckert number Ec.

6. Concluding remarks

Effects of electric and magnetic fields in the boundary layer flow of Williamson fluid over an unsteady stretching surface are analyzed. The presented analysis leads to the following main results:

- The magnetic parameter M, Weissenberg number We and suction parameter A attain the maximum velocity at $\eta = 0$ and the velocity decreases most rapidly with the increasing values of η.
- Momentum and thermal boundary layer thickness decrease with an increase in suction parameter A.
- Influence of Weissenberg number We, suction parameter A, unsteadiness parameter S and the electric parameter E_1 on temperature profile $\theta(\eta)$ is qualitatively similar.
- Effects of E_1 and Pr on temperature profile $\theta(\eta)$ are quite opposite.
- Velocity field $f'(\eta)$ is a decreasing function of magnetic parameter M whereas the temperature profile $\theta(\eta)$ is an increasing function of magnetic parameter M.
- An increase in suction parameter A, unsteadiness parameter S and magnetic parameter M enhances the skin friction coefficient $Re_x^{1/2}C_f$ while the increase in Weissenberg number We and electric parameter E_1 decreases the skin friction coefficient $Re_x^{1/2}C_f$.
- The local Nusselt number increases for larger suction parameter A, unsteadiness parameter S, electric parameter E_1 and Prandtl number Pr.

References

[1] H. Alfven, Existence of electromagnetic-hydrodynamic waves, Nature 150 (1942) 405–406.
[2] J. Hartmann, I. Hg-Dynamics, Theory of the laminar flow of an electrically conducting liquid in a homogeneous magnetic field, K. Dan. Vidensk. Selsk. Mat.-Fys. Medd. 15 (1937) 1–27.
[3] M.M. Rashidi, S. Abelman, N.F. Mehr, Entropy generation in steady MHD flow due to a rotating disk in a nanofluid, Int. J. Heat Mass Transfer 62 (2013) 515–525.
[4] S.A. Shehzad, A. Alsaedi, T. Hayat, Hydromagnetic steady flow of Maxwell fluid over a bidirectional stretching surface with prescribed surface temperature and prescribed surface heat flux, Plos One 8 (7) (2013) e68139.
[5] M. Turkyilmazoglu, Exact solutions for the incompressible viscous magnetohydrodynamic fluid of a rotating disk flow, Int. J. Nonlinear Mech. 46 (2011) 306–311.
[6] T. Hayat, S.A. Shehzad, M.B. Ashraf, A. Alsaedi, Magnetohydrodynamic mixed convection flow of thixotropic fluid with thermophoresis and Joule heating, J. Thermophys. Heat Transfer 27 (2013) 733–740.
[7] M. Sheikholeslami, M. Gorji-Bandpay, D.D. Ganji, Magnetic field effects on natural convection around a horizontal circular cylinder inside a square enclosure filled with nanofluid, Int. Commun. Heat Mass Transfer 39 (2012) 978–986.
[8] B.S. Dandapat, A. Mukhopadhyay, Finite amplitude long wave instability of a film of conducting fluid flowing down an inclined plane in presence of electromagnetic field, Int. J. Appl. Mech. Eng. 8 (2003) 379–383.
[9] T. Hayat, A. Shafiq, M. Nawaz, A. Alsaedi, MHD axisymmetric flow of third grade fluid between porous disks with heat transfer, Appl. Math. Mech. 33 (6) (2012) 749–764.
[10] K. Ahmad, R. Nazar, Unsteady magnetohydrodynamic mixed convection stagnation point flow of a viscoelastic fluid on a vertical surface, JQMA 6 (2) (2010) 105–117.
[11] M. Hatami, M. Sheikholeslami, M. Hosseini, D.D. Ganji, Analytical investigation of MHD nanofluid flow in non-parallel walls, J. Mol. Liq. 194 (2014) 251–259.
[12] M. Sheikholeslami, D.D. Ganji, M. Gorji-Bandpy, S. Soleimani, Magnetic field effect on nanofluid flow and heat transfer using KKL model, J. Taiwan Inst. Chem. Eng. 45 (2014) 795–807.
[13] M.H. Abolbashari, N. Freidoonimehr, F. Nazari, M.M. Rashidi, Entropy analysis for and unsteady MHD flow past a stretching permeable surface in nanofluid, Powder Technol. 267 (2014) 256–267.
[14] M.M. Rashidi, E. Erfani, Analytical method for solving steady MHD convective and slip flow due to a rotating disk with viscous dissipation and Ohmic heating, Eng. Comput. 29 (6) (2012) 562–579.
[15] M.M. Rashidi, M. Ali, N. Freidoonimehr, B. Rostami, M.A. Hossain, Mixed convective heat transfer for MHD viscoelastic fluid flow over a porous wedge with thermal radiation, Adv. Mech. Eng. (2014) 10.
[16] K. Bhattacharyya, S. Mukhopadhyay, G.C. Layek, I. Pop, Effects of thermal radiation on micropolar fluid flow and heat transfer over a porous shrinking sheet, Int. J. Heat Mass Transfer 55 (2012) 2945–2952.
[17] O.D. Makinde, A. Ogulu, The effect of thermal radiation on the heat and mass transfer flow of a variable viscosity fluid past a vertical porous plate permeated by a transverse magnetic field, Chem. Eng. Commun. 195 (2008) 1575–1584.
[18] T. Hayat, A. Shafiq, A. Alsaedi, Effect of Joule heating and thermal radiation in flow of third-grade fluid over radiative surface, Plos One 9 (1) (2014) e83153.
[19] T.G. Motsumi, O.D. Makinde, Effects of thermal radiation and viscous dissipation on boundary layer flow of nanofluids over a permeable moving flat plate, Phys. Scr. 86 (2012) 045003.
[20] O.D. Makinde, MHD mixed-convection interaction with thermal radiation and nth order chemical reaction past a vertical porous plate embedded in a porous medium, Chem. Eng. Commun. 198 (2011) 590–608.
[21] S.A. Shehzad, A. Alsaedi, T. Hayat, M.S. Alhuthali, Thermophoresis particle deposition in mixed convection three-dimensional radiative flow of an Oldroyd-B fluid, J. Taiwan Inst. Chem. Eng. 45 (2014) 787–794.
[22] S.J. Liao, Notes on the homotopy analysis method: Some definitions and theorems, Commun. Nonlinear Sci. Numer. Simul. 14 (2009) 983–997.
[23] S.J. Liao, Homotopy Analysis Method in Nonlinear Differential Equations, Springer & HigherEducation Press, 2012.
[24] T. Hayat, M. Farooq, A. Alsaedi, Z. Iqbal, Melting heat transfer in the stagnation-point flow of Powell-Eyring fluid, J. Thermophys. Heat Transfer 27 (2013) 761–766.
[25] I.C. Mandal, S. Mukhopadhyay, Heat transfer analysis for fluid flow over an exponentially stretching porous sheet with surface heat flux in porous medium, Ain Shams Eng. J. 4 (2013) 103–110.
[26] S.S. Motsa, P. Sibanda, F.G. Awad, S. Shateyi, A new spectral homotopy analysis method for the MHD Jeffery Hamel problem, Comput. Fluids 39 (2010) 1219–1225.
[27] T. Hayat, A. Shafiq, M. Nawaz, A. Alsaedi, MHD axisymmetric flow of third-grade fluid between porous disks with heat transfer, Appl. Math. Mech. Engl. Ed. 33 (6) (2012) 749–764.
[28] R. Ramzan, M. Farooq, A. Alsaedi, T. Hayat, MHD three dimensional flow of couple stress fluid with Newtonian heating, Eur. Phys. J. Plus 128 (2013) 49.

[29] M.M. Rashidi, S.A.M. Pour, T. Hayat, S. Obaidat, Analytic approximate solutions for steady flow over a rotating disk in porous medium with heat transfer by homotopy analysis method, Comput. Fluids 54 (2012) 1–9.
[30] M. Mustafa, T. Hayat, S. Obaidat, Stagnation-point flow and heat transfer of a Casson fluid towards a stretching sheet, Z. Naturforsch. 67 (2012) 70–76.
[31] S. Kazem, S. Abbasbandy, S. Kumar, Fractional-order Legendre functions for solving fractional-order differential equations, Appl. Math. Modell. 37 (2013) 5498–5510.
[32] T. Hayat, Z. Hussain, M. Farooq, A. Alsaedi, M. Obaid, Thermally stratified stagnation point flow of an Oldroyd-B fluid, Int. J. Nonlinear Sci. Numer. Simul. 15 (2014) 77–86.
[33] T. Hayat, Y. Saeed, S. Asad, A. Alsaedi, Soret and Dufour effects in the flow of Williamson fluid over an unsteady stretching surface with thermal Radiation, Z. Naturforsch. 70 (2015) 235–243.
[34] P.O. Olanrewaju, Effects of internal heat generation on hydromagnetic non-Darcy flow and heat transfer over a stretching sheet in the presence of thermal radiation and Ohmic dissipation, World Appl. Sci. J. 16 (2012) 37–45.